SCIENTIFIC REPORTS
nature research

Check for updates

OPEN

Anchoring the Late Devonian mass extinction in absolute time by integrating climatic controls and radio-isotopic dating

Anne-Christine Da Silva[1]✉, Matthias Sinnesael[2], Philippe Claeys[3], Joshua H. F. L. Davies[4], Niels J. de Winter[3,5], L. M. E. Percival[3], Urs Schaltegger[6] & David De Vleeschouwer[7]✉

The Devonian Frasnian–Famennian (F–F) boundary marks one of the five main extinction intervals of the Phanerozoic Aeon. This time was characterized by two pulses of oceanic anoxia, named the Lower and Upper Kellwasser events, during which massive marine biodiversity losses occurred. This paper presents high-resolution magnetic susceptibility, X-ray fluorescence elemental geochemistry and carbon isotope datasets obtained from the Steinbruch Schmidt F–F boundary section (Germany). These records lead to an astronomical time calibration of the environmental changes associated with the two ocean anoxia pulses. Cyclostratigraphic interpretation indicates deposition of the black argillaceous Lower and Upper Kellwasser horizons over ~ 90 and ~ 110 kyr, respectively; approximately equivalent to the duration of one short eccentricity cycle. This study confirms that the succession of events within the Upper Kellwasser event is paced by obliquity, under a low-eccentricity orbit. Hence, astronomical insolation forcing likely contributed to the expansion of ocean anoxia and other environmental perturbations associated with these two crises. The new floating chronology established for the Steinbruch Schmidt section is anchored in numerical time by means of a radio-isotopic date, obtained from a bentonite layer interbedded between the two Kellwasser horizons. After anchoring, this time scale gives a high-precision age of 371.870 ± 0.108 Ma for the F–F boundary.

The Devonian Period experienced several episodes of strong environmental and climate changes, including different pulses of extinction and global carbon-cycle perturbations. The Frasnian–Famennian (F–F) boundary event stands out among these Devonian environmental perturbations, due to its strong impact on marine ecosystems [e.g.1] and is considered as one of the "Big Five" major Phanerozoic mass extinctions according to a recent synthesis and reappraisal by[1]. Classically, the sedimentary expression below and at the F–F boundary, consists of two dark shale intervals, referred to as the Lower and Upper Kellwasser shales respectively (LKW, UKW, overview in[2]). These dark shales stratigraphically correspond to two distinct positive carbon-isotope ($\delta^{13}C$) excursions recorded around the globe, including at locations where black shales did not develop[3–6]. The origin of the extinction and its specific timing have been debated for a long time. Suggested causal mechanisms for the extinction include one or more extraterrestrial impacts[7,8], large-scale volcanism[9,10], either climate cooling[11] or warming[12], and enhanced continental weathering, through mountain building[13] or development of terrestrial forests[5,14]. Increase continental weathering in particular would have resulted in eutrophication, planktonic algal blooming and subsequent widespread marine anoxia.

[1]Sedimentary Petrology Laboratory, Liège University, Allée du Six Août, 12, 4000 Liège, Belgium. [2]Department of Earth Sciences, Mountjoy Site, Durham University, South Road, Durham DH1 3LE, UK. [3]Analytical, Environmental and Geo-Chemistry (AMGC), Vrije Universiteit Brussel, Pleinlaan 2, 1050 Brussels, Belgium. [4]Département des sciences de la terre et de l'atmosphere, Université du Québec à Montréal, Montréal, Canada. [5]Department of Earth Sciences, Faculty of Geosciences, Utrecht University, Princetonlaan 8a, 3584 CB Utrecht, The Netherlands. [6]Département des sciences de la terre, Université de Genève, 1205 Geneva, Switzerland. [7]MARUM—Center for Marine Environmental Sciences, University of Bremen, Leobenerstraße, 28359 Bremen, Germany. ✉email: ac.dasilva@uliege.be; ddevleeschouwer@marum.de

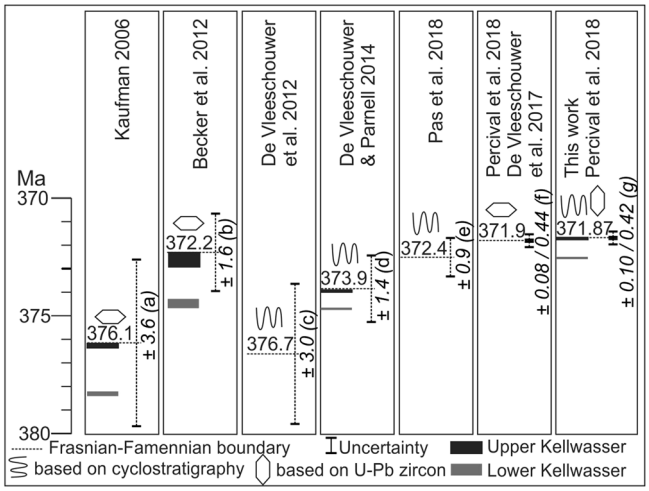

Figure 1. Frasnian–Famennian time scales and their uncertainties proposed in recent studies. (**a**) Uncertainty based on the 2σ error of each individual ash bed with an additional uncertainty of 2 Ma and error channel propagation age. (**b**) Uncertainty based on smoothing spline procedure with a smoothing factor of 0.45[15]. (**c**) Uncertainty based on a counting error of 1 long eccentricity cycle to the existing error bar of[16]. (**d**) Uncertainty based on Baysian age-depth Bchron model[53]. (**e**) Uncertainty includes uncertainty on the stratigraphic position of the F–F boundary, transferred in time through estimated sedimentation rate, plus one long eccentricity cycle, plus the uncertainty on the Devonian-Carboniferous boundary[22]. This uncertainty may be under evaluated, since it is based on an extrapolation from an ash beds 13.5 Myr younger than the F–F boundary. (**f**) Uncertainty based on the ash bed[25] (372.360 ± 0.053 Ma) and extrapolation astrochronology model from[6]. (**g**) Uncertainty based on the uncertainty from the ash bed of[25] and uncertainties obtained by comparing the different astrochronologic estimates in this paper.

Better constraints on the rate and timing of environmental change before, during and after the extinction could resolve the diverging hypotheses. Indeed, numerous different chronologies have been constructed for the F–F extinction event (synthesis in Fig. 1). Duration estimates of the interval between the onset of the first anoxic event (LKW) and the F–F boundary range between 800 and ~ 2,500 kyr, as presented below:

1. The ~ 2,500 kyr estimate[15,16] is primarily based on three ash beds dated by U–Pb as middle Frasnian to late Famennian in age. These are the Belpre Ash [USA, 379.5 ± 1.17 Ma in the Geological Time Scale (GTS) 2012[17], originally published by[18]], the bentonite from the Steinbruch Schmidt section [Germany, 373.68 ± 1.49 Ma in GTS 2012[17], originally published by[19]], and a bentonite in the Piskahegan Group (Canada, 364.08 ± 2.2 Ma in GTS2012[17], originally published by[18]). The large error bars on each of these individual radio-isotopic dates and also the use of non-chemically abraded U–Pb ages leads to substantial uncertainty, and potential inaccuracy on this ~ 2,500 kyr duration estimate.
2. Recently, strong efforts have been made to improve the Devonian time scale through cyclostratigraphy[20–22]. For the F–F interval, De Vleeschouwer et al.[23] worked on the expression of Milankovitch cycles in the Kowala section in Poland and suggested a ~ 800 kyr time-gap between the onsets of the LKW and the UKW and a ~ 400 kyr duration for low oxygen levels during the UKW. Subsequently, De Vleeschouwer et al.[6] complemented the Kowala section, with sections from Canada, U.S.A., China and Belgium compiled into a global cyclostratigraphic framework that places the onset of the positive LKW $\delta^{13}C$ excursion ~ 800 kyr before the F–F boundary.
3. Pas et al.[22] proposed a cyclostratigraphic framework for the whole Famennian through different cores from the Illinois Basin, anchored to a precise Famennian–Tournaisian boundary age based on U–Pb dating of uppermost Famennian bentonites from Poland[24]. This cyclostratigraphic approach resulted in a F–F boundary age of 372.4 Ma ± 0.9 Myr. No duration is proposed for the interval between the LKW and UKW. The F–F age is based on a cyclostratigraphic extrapolation from ash beds 13.5 Myr younger than the F–F boundary.
4. Recently, Percival et al.[25] re-dated zircons from the Steinbruch Schmidt ash bed located between the LKW and UKW (utilizing modern chemical abrasion isotope dilution thermal ionization mass spectrometry (CA-ID-TIMS) U–Pb geochronology techniques as well as the Earthtime spike solutions), generating a new age of 372.360 ± 0.053 Ma for the bentonite. Using this age, extrapolating the De Vleeschouwer et al.[6] cyclostratigraphic framework and assuming a constant sedimentation rate for the limestones deposited between the two Kellwasser horizons the F–F boundary age was estimated to be between 371.93 and 371.78 Ma[25].

The present study brings together the latest developments in the fields of astrochronology and radio-isotopic dating to conduct a cyclostratigraphic analysis of a multi-proxy data set for the Steinbruch Schmidt section. It subsequently integrates the high-precision radio-isotopic date[25] to tie the floating chronology to an absolute

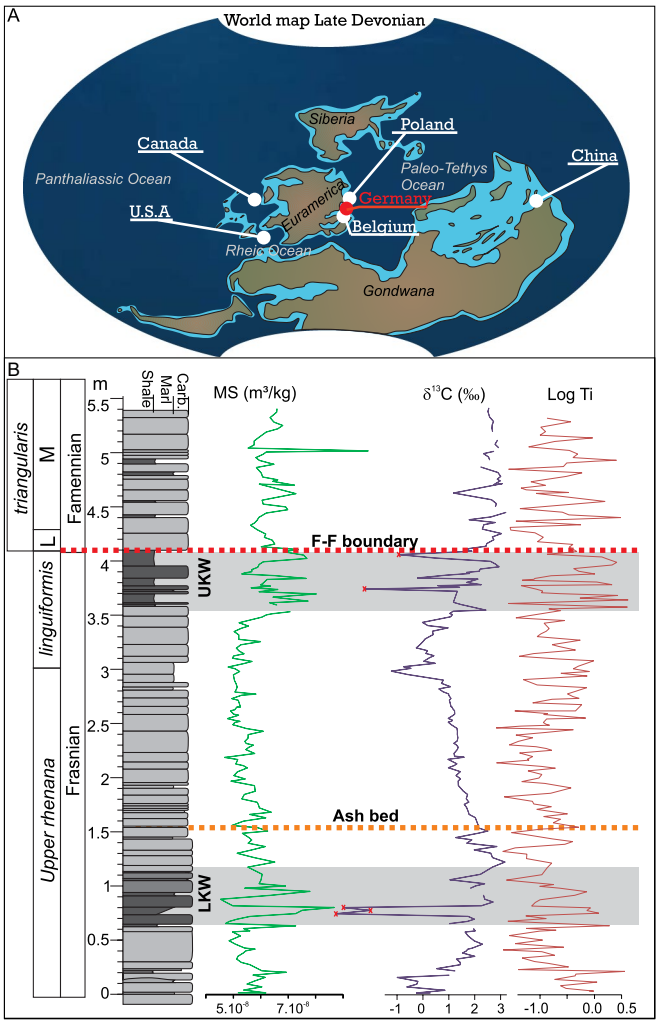

Figure 2. Geological Setting and lithological column of the Steinbruch Schmidt section and of other records used in this paper. (**A**) World map of Late Devonian, modified after[54], with location (in red) of the Steinbruch Schmidt section (Germany) and other records for comparison (in grey): Fuhe (China), Kowala (Poland), Sinsin (Belgium), Section C (Western Canada), and CG-1 and H-32 from Iowa (U.S.A.). (**B**) Lithological column from Steinbruch Schmidt section, modified from[27] and conodont biostratigraphy from[28], with magnetic susceptibility (MS), carbon isotopes ($\delta^{13}C$) and logTi depth-series. In the $\delta^{13}C$ record, outliers with the extreme low values, marked with red crosses, are considered as diagenetically altered and were removed for spectral analysis. The Frasnian–Famennian (F–F) boundary is marked by a dotted red line, the ash bed dated by[25] by dotted orange line, and the lower and upper Kellwasser (LWK, UKW) black shale intervals are underlined by grey areas.

time frame. These results are then compared with previous chronologies. This approach leads to a unique high precision chronology for the F–F interval, anchored in absolute time and at unprecedented resolution.

Geological setting, data and methods

The Steinbruch Schmidt section was deposited at tropical palaeolatitudes (Fig. 2A) on a submarine rise, below the wave action zone, in a quiet and poorly oxygenated setting with the LKW and UKW corresponding to the deepest settings preserved[26]. This section offers outstanding conditions for a stratigraphic framework and timescale that can be globally correlated. It contains well-developed Lower and Upper Kellwasser black-shale intervals and associated positive carbon-isotope excursions[3,27], a high-precision radio-isotopic date[19,25], as well as an excellent biostratigraphic framework[28]. For this study, the 5.3 m of outcropping section, which ranges from 65 cm below the LKW to 75 cm above the UKW (Fig. 2B, N = 264) was sampled at high-resolution (2 cm) and each sample was measured for magnetic susceptibility, carbon isotopes and XRF geochemistry, following the protocol below. As mentioned above, there is an ash bed in the Steinbruch Schmidt section, intercalated between the two Kellwasser horizons. The "Bed 36" ash occurs 1.5 m higher than the base of our sampling interval and 2.5 m below the F–F boundary, and was recently re-dated by[25] to 372.360 ± 0.053 Ma.

Magnetic susceptibility was measured 3 times on each sample, with a KLY-3 (AGICO Kappabridge) at Liège University (Belgium), averaged and weighted to produce mass-specific (m^3/kg) data. At the Vrije Universiteit

Spectral techniques	Record	Sed rate boundaries (cm/kyr)	Duration of whole record (kyr)	Sed rate (cm/kyr)	Duration of interval between LKW and F-F (kyr)	Difference with median (kyr)	Difference with ORTA MS (kyr)
eTimeOpt_Prec_SE	MS	0.1–0.55	1,062	0.50	694.0	11.0	16.0
eTimeOpt_SE_LE	MS	0.1–0.55	1,085	0.49	697.5	12.0	39.0
eTimeOpt_Prec_SE	LogTi	0.1–0.55	1,007	0.53	716.0	66.0	39.0
eTimeOpt_SE_LE	LogTi	0.1–0.55	1,124	0.47	812.0	51.0	78.0
eTimeOpt_Prec_SE	$\delta^{13}C$	0.1–0.55	1,129	0.47	708.0	56.0	83.0
eTimeOpt_SE_LE	$\delta^{13}C$	0.1–0.55	1,100	0.48	743.0	27.0	54.0
ORTA	MS		1,046	0.51	775.0	27.0	0.0
ORTA	LogTi		1,073	0.49	843.0	0.0	27.0
ORTA	$\delta^{13}C$		994	0.53	809.0	79.0	52.0
			Median	**Median**	**Median**	**Average**	**Average**
			1,073.0	0.49	743.00	36.6	43.1
		Standard deviation	47.31	0.02	56.14		

Table 1. Results obtained by different spectral analysis techniques on different proxies on the Steinbruch Schmidt section. Spectral techniques include eTimeOpt_Prec_SE, corresponding to the eTimeOpt technique focussing on the modulation of precession by short eccentricity; eTimeOpt_SE_LE, corresponding to the eTimeOpt technique focussing on the modulation of short eccentricity by long eccentricity and ORTA Optimized Relative Timing Approach. Records includes magnetic susceptibility (MS), Log Ti and Carbon isotopes ($\delta^{13}C$). Results are expressed as the duration of the whole record in kyr, sedimentation rate (SedRate in cm/kyr), duration of the interval between the onset of the Lower Kellwasser (LKW) Carbon isotopic excursion and Frasnian–Famennian (F–F) boundary; and difference with median value.

Brussel (Belgium), a Bruker M4 Tornado, operated under near-vacuum conditions (20 mbar) was used for the µXRF measurements. The conditions used were: a 30 W Rh anode metal-ceramic X-ray tube and a 30 mm^2 SSD with a resolution of 145 eV (Mn–Ka). The X-ray beam was focused by a poly-capillary lens on a spot with a diameter of 25 mm (Mo–Ka). An integration time of 60 s per point was chosen, satisfying the conditions for reaching the Time of Stable Accuracy and Time of Stable Reproducibility and providing the ideal compromise between high analytical accuracy and precision and high sample throughput ([29] for analytical details). The carbon ($\delta^{13}C$) stable isotope ratios of bulk powered carbonate material were also determined at the Vrije Universiteit Brussel, using a NuPerspective isotope ratio mass spectrometer (IRMS) interfaced with a NuCarb automated carbonate device. Acidification of the samples took place at a temperature of 70 °C. All values are expressed relative to the Vienna Pee Dee Belemnite (‰VPDB) standard. Calibration was carried out using an in-house Marbella limestone (MAR) standard (+3.41 ‰VPDB) calibrated against the international NBS-19 standard[30]. On the basis of replicated measurements of the MAR standard, reproducibility errors on $\delta^{13}C$ are < 0.05 ‰ (1 σ).

All time-series analyses are performed on the R platform[31]. All proxy series are interpolated to 0.02 m. First, the function eTimeOpt within the *Astrochron* package[32] is used to evaluate sedimentation rates and their stratigraphic evolution[33,34]. The eTimeOpt method provides a quantitative assessment of a sequence of possible sedimentation rates, adopting a sliding window approach. Within each window, sedimentation rates that result in precession amplitude modulation patterns and frequency ratios in accord with astronomical theory are singled out. The eTimeOpt function requires the user to provide target eccentricity and precession periodicities to be tested. For the Devonian, this requires non-trivial assumptions, as the periodicities of obliquity and precession in "deep time" are affected by the tidal dissipation of energy. The precession periodicities (16.85, 19.95 kyr) as calculated by[35] are selected. Long and short eccentricity relate to the shape of Earth's orbit and not to its rotational speed, hence eccentricity is not affected by tidal dissipation. Therefore, the 100 kyr and 405 kyr periodicities have remained unchanged throughout geological history. Numerical calculations by Laskar et al.[36,37] have demonstrated the extraordinary stability of the periodicity of the 405 kyr term, often referred to as the metronome of the Phanerozoic. In this study, eccentricity periodicities of 94.9, 98.9, 123.8, 130.7 and 405 kyr are adopted[37].

The eTimeOpt chronology is then compared with a time scale obtained though the age modelling protocol designed by[6]. These authors correlated 6 globally-distributed Frasnian–Famennian sections (Poland, Kowala section; western Canada, Section C; Iowa, H-32 and CG-1 drill core; Belgium, Sinsin section; and South China, Fuhe section, Fig. 2A), through tie-points obtained by visually correlating distinct features in the stratigraphic trends of magnetic susceptibility and carbon-isotope compositions, whilst respecting conodont biostratigraphy constraints. A tentative relative age was assigned to each of those tie-points, abiding to the 405 kyr astrochronologic framework for Western Canada (Fig. 7 in[6]). Those authors then applied a Monte Carlo procedure that distorts time-differences between consecutive tie-points, i.e. small-scale stretching and squeezing between tie points. Their goal was to reach the best expression of the Milankovitch cycles, under the presumption that the chronology with the clearest orbital signature advocated to be the most accurate (detailed description in[6]). This technique is called the Optimized Relative Timing Approach (ORTA). The new results from the Steinbruch Schmidt section are incorporated into this correlation framework and assigned relative age tie-points (with 0 kyr corresponding to the F–F boundary) identical to those in[6].

Finally, the Wavelet Transform evolutive spectra (CWT[38]), obtained through the biwavelet package[39] is applied. Continuous wavelet is an evolutive spectral techniques that reveals the evolution of periodicities for

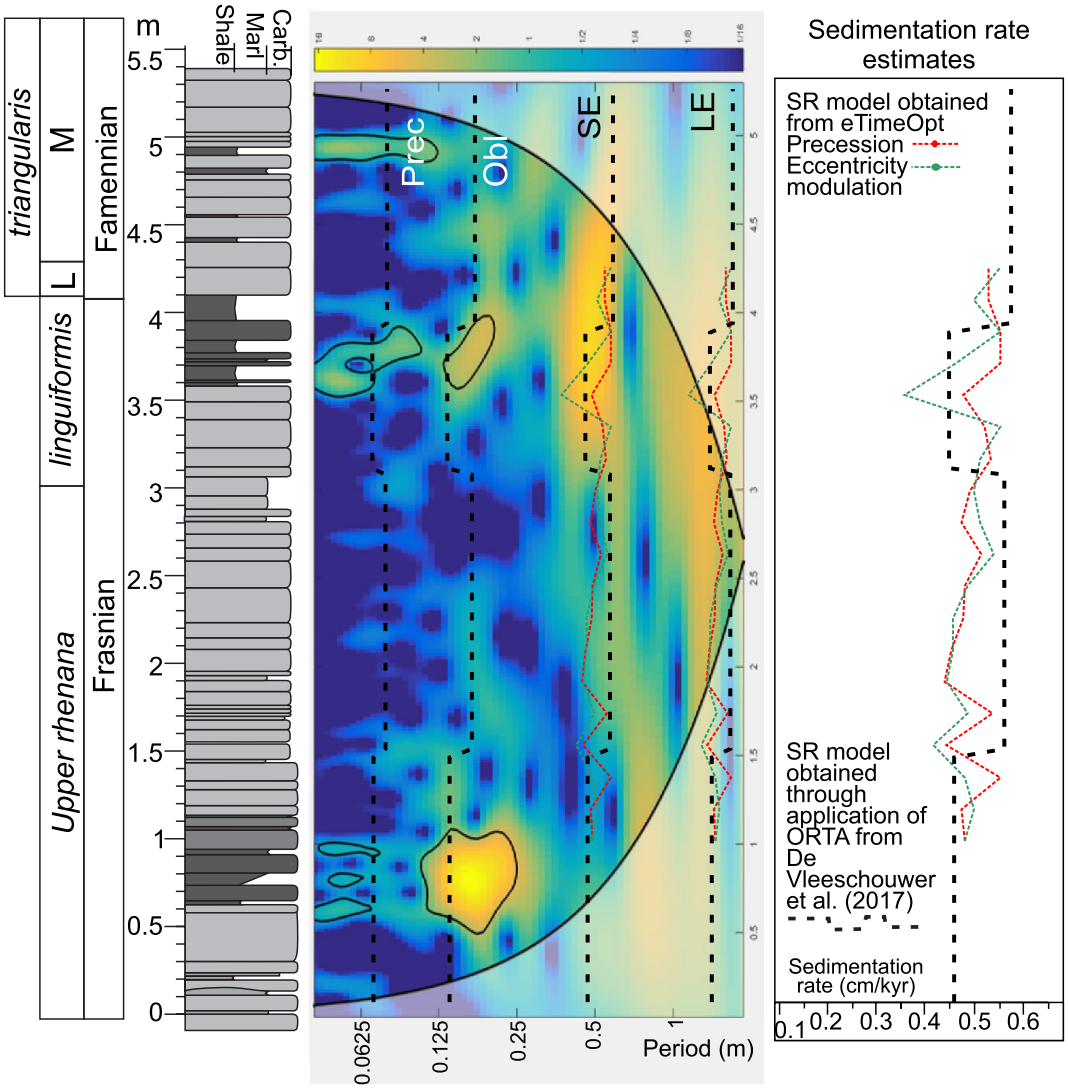

Figure 3. Continuous Wavelet Transform of the Magnetic susceptibility signal, together with the different results from eTimeOpt (red and green lines) and ORTA (black dotted line) on the magnetic susceptibility record. *LE* long eccentricity, *SE* short eccentricity, *Obl* obliquity, *Prec* precession.

the studied sections and detects changes in cycle thickness and, hence, sediment accumulation rate. These CWT results are compared with the results from eTimeOpt and ORTA.

Results

Magnetic susceptibility, logTi and $\delta^{13}C$ are selected as proxies for the section (Fig. 2B). Magnetic susceptibility (MS) is viewed as a proxy for detrital input e.g.[40], logTi to reflect the relative rate of siliciclastic sedimentation[41,42], and carbon-isotope variations as indications for net changes in the carbon cycling between the ocean, atmosphere, biosphere and lithosphere[43]. Ti evolution includes very strong peaks. By using the logarithmic signal, modest base-level variations are enhanced while positive peak values are reduced. The Steinbruch Schmidt section is dominated by carbonate lithologies, with the two Kellwasser dark marls or shales. Within these argillaceous intervals, MS increases. Although the LKW dark marly layer ranges between 0.6 and 1.15 m, the carbon isotope ratios start to increase at 0.15 m, reach a peak around 1.2 m and then decreases until about 3 m. The UKW marly dark layer ranges between 3.6 and 4.1 m with the carbon isotope ratios increasing from 3 m. LogTi values display strong variations, with a slight increase in the average value during the marly Kellwasser intervals.

The application of eTimeOpt produces a first assessment of a potential Milankovitch imprint in these different proxy records. As an input parameter, eTimeOpt requires an estimate of a range of plausible sedimentation rates for the studied interval. As outlined in the introduction, LKW-to-F–F-boundary duration estimates range from 800 kyr[6] to more than three times that timespan[15]. The corresponding stratigraphic interval at the Steinbruch Schmidt section consists of about 400 cm of section. Hence, plausible sedimentation rates range between 0.17 and 0.5 cm/kyr. The eTimeOpt approach is applied to these different records (logTi, MS and $\delta^{13}C$) with a grid of 100 sedimentation rates between 0.15 and 0.55 cm/kyr range. The results of eTimOpt for amplitude modulation

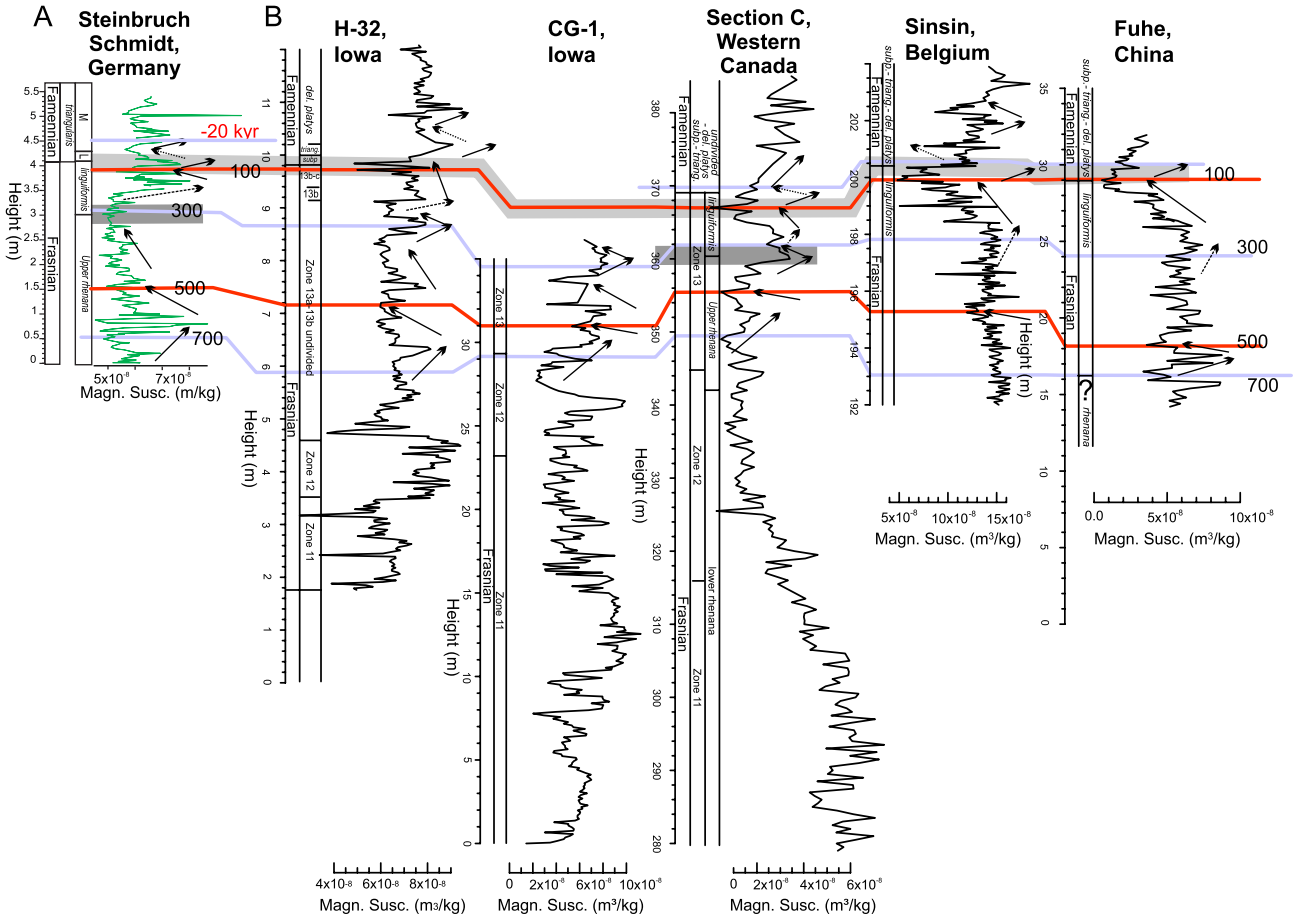

Figure 4. Magnetic susceptibility correlation of Steinbruch Schmidt section with other F–F records (H-32, CG-1, Section C, Sinsin, and Fuhe, see[6]) and visual distinct magnetic susceptibility features for correlations (red lines and arrows). These tie points have to respect the biostratigraphic constraints (underlined by grey area) and carbon isotope correlations (Fig. 5, blue lines). The black numbers are ages assigned to each tie-point, according to the existing astrochronologic framework of Section C and Kowala[23,55]. *Fam.* Famennian, *h.-j.* hassi-jamieae, *U.* upper, *linguif.* linguiformis, *subp.* subperlobata, *triang.* triangularis, *del.* platys delicatula platys.

of precession, give evolving sedimentation rates (for LogTi, MS and $\delta^{13}C$) ranging in average values between 0.47 and 0.53 cm/kyr (Table 1, Fig. 3, Fig. Suppl. Mat. 1).

These different eTimeOpt assessments provide total duration estimates for the studied interval (Table 1) of 1,129 kyr ($\delta^{13}C$), 1,062 kyr (MS) and 1,007 kyr (logTi). However, eTimeOpt for amplitude modulation of precession cannot consider the full sedimentation rate interval as the proxy-series resolution is too low to resolve precession cycles for sedimentation rates lower than 0.26 cm/kyr. Running eTimeOpt again on all proxies, investigating the amplitude modulation of short eccentricity by long eccentricity circumvents this problem. These settings lead to eTimeOpt results for the full sedimentation rate range. Despite the fundamentally different eTimeOpt settings, the sedimentation rates remain similar (ranging between 0.47 to 0.49 cm/kyr, Table 1, Fig. 3, Fig. Suppl. Mat. 1), which translate into duration estimates of 1,100 kyr ($\delta^{13}C$), 1,085 kyr (MS) and 1,124 kyr (logTi) for the whole section (Table 1). The eTimeOpt results appear thus consistent, for both amplitude modulation of precession by short eccentricity or short eccentricity by long eccentricity. Furthermore, the eTimeOpt results point to a relatively short duration between the base of the LKW $\delta^{13}C$ excursion and the F–F boundary, ranging between 694 and 812 kyr, which confirms the rather short LKW-to-F–F-boundary duration estimates by[6].

Next, Steinbruch Schmidt proxy records are placed within the ORTA framework developed by De Vleeschouwer et al.[6] A correlation between the Steinbruch Schmidt record and the six records from[6] is established by identifying five correlation tie-points based on biostratigraphy, $\delta^{13}C$ chemostratigraphy, and magnetic susceptibility proxy records (Figs. 4, 5). The decrease in the amount of tie points (from 7 to 5) compared to[6] gives more freedom for distortions. The five tie-points are assigned tentative relative ages with respect to the F–F boundary of − 20 kyr (above the boundary), 100 kyr, 300 kyr, 500 kyr and 700 kyr (below the boundary, Figs. 4, 5), as prescribed for the ORTA procedure. The 720 kyr that separate the extreme tie points dictate a mean sedimentation rate of 0.55 cm/kyr, only slightly higher than the sedimentation rates obtained through eTimeOpt. The ORTA transforms the signal from the distance to the time domain between the different tie-points using a Monte Carlo approach, retaining the chronology that has the best expression of the expected Milankovitch frequencies between all different proxies. The algorithm yields an optimized result with a total duration of 1,045 ka, corresponding to

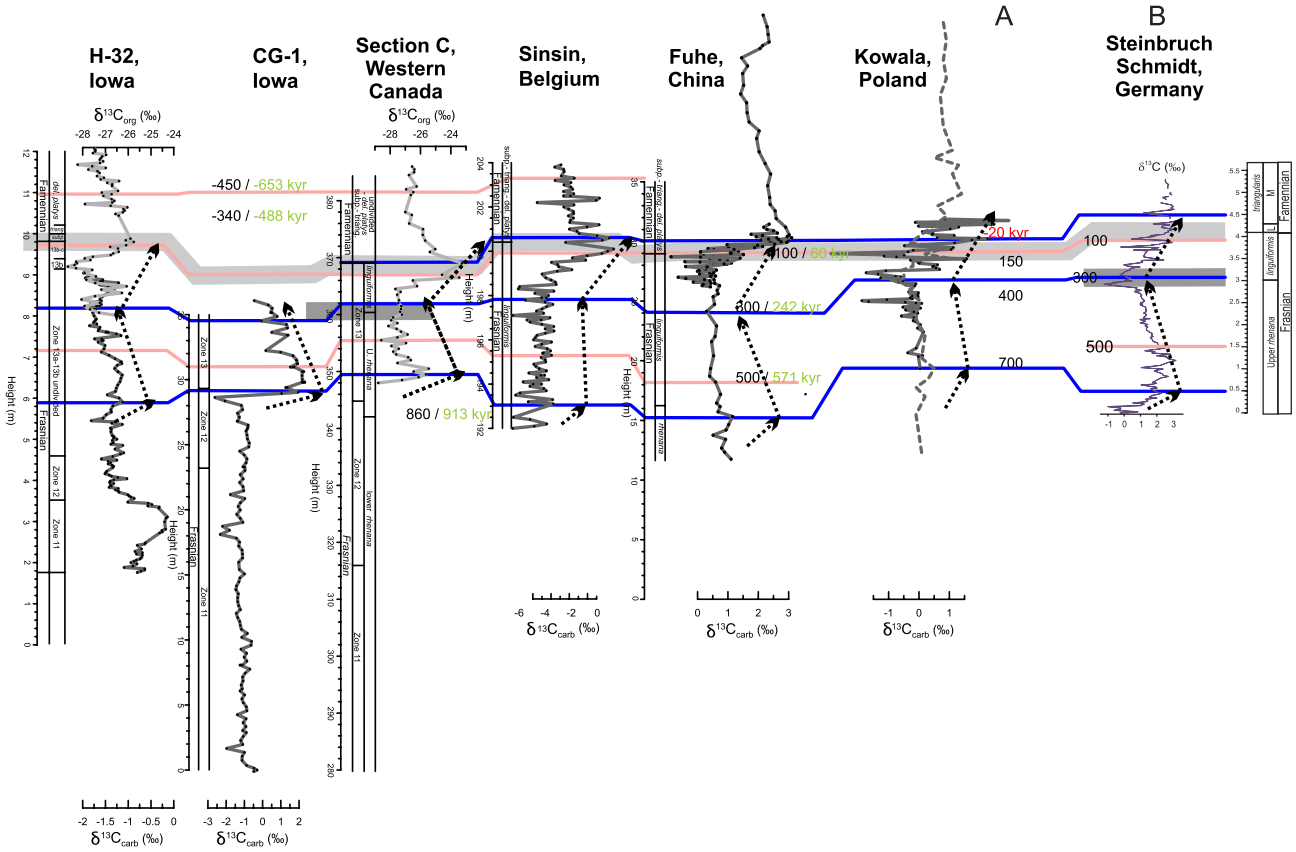

Figure 5. Carbon isotope correlation of Steinbruch Schmidt section with other F–F records (H-32, CG-1, Section C, Sinsin, Fuhe, and Kowala, see[6]) obtained by visually correlating distinct features in carbon isotope geochemistry (blue ties and dotted arrows). These tie points are accepted only if they respect the biostratigraphic constraints (underlined by grey area) and magnetic susceptibility correlations (Fig. 4, red lines). The black numbers are ages assigned to each tie-point, according to the existing astrochronologic framework of Section C and Kowala[23,55]. Abbreviations as in Fig. 4.

a mean sedimentation rate of 0.51 cm/kyr for magnetic susceptibility, as well as 1,073 kyr and 0.49 cm/kyr for LogTi and 1,046 and 0.49 cm/kyr (Table 1). This result fall close to those obtained through eTimeOpt. Finally, the results are examined using a continuous wavelet transform (Fig. 3, Fig. Suppl. Mat. 1), which shows strong spectral power at periods of 0.4–0.7 and 1.5–2 m. These periods fit respectively with short and long eccentricity, with sedimentation rates around 0.5 cm/kyr; they fully agree with the results from eTimeOpt and ORTA (Table 1).

Two fully independent spectral techniques (eTimeOpt from[33], and the ORTA from[6]) applied on the different proxies from the Steinbruch Schmidt section, lead to similar results for the duration of the whole section. These duration estimates for the section range between a minimum of 994 kyr to a maximum value of 1,129 kyr (Table 1), whilst duration of the interval between the beginning of the $\delta^{13}C$ excursion and the F–F boundary ranges between 694 and 843 kyr. The narrow range of results is also illustrated by the average difference between different duration estimates and the median estimate of only 37 kyr (Table 1).

Discussion

The subsequent discussion is primarily based on the results obtained by ORTA. The focus lies on ORTA from the magnetic susceptibility result for the following reasons (Fig. 3, Fig. Suppl. Mat. 1): (1) eTimeOpt is an evolutive technique that works with sliding windows. Results are reported for window mid-points, which implies that the results for the extremities of the record need to be extrapolated. (2) For the lower and upper Kellwasser black shales, a rather low sedimentation rate is expected[44], which is indeed the case with ORTA on Magnetic susceptibility, but not with eTimeOpt or on ORTA on other proxies. (3) The results from ORTA exhibit a slightly better fit with the band of strong power in the continuous wavelet transform and evolutive harmonic analysis. Nevertheless, all results are very close as the difference between the various results obtained through the different techniques and those from ORTA on magnetic susceptibility never amounts to more than 83 kyr (Table 1). The Supplementary Materials shows other results from eTimeOpt and from ORTA on all proxies in details (Figs. Suppl. Mat. 1–3), but the outcomes are similar and the slight differences between the models will be discussed and integrated.

The Steinbruch Schmidt bentonite layer at bed 36, located between the LKW and the UKW horizons has been recently re-dated by[25], who reported a weighted mean age of 372.360 ± 0.053 Ma. Combining this age with the present cyclostratigraphy provides an integrated time scale for the Frasnian–Famennian boundary interval

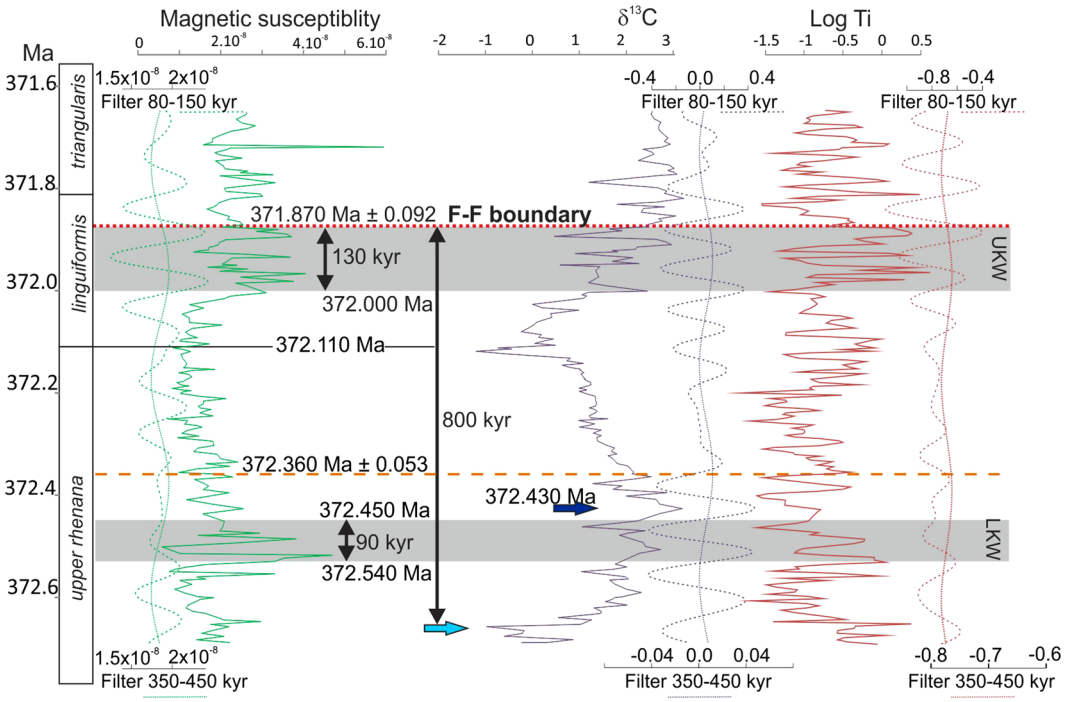

Figure 6. Integrated anchored chronology for the Frasnian–Famennian boundary, obtained through the combination of ORTA and the[25] radio-isotopic date (orange dotted line). The grey bands mark the extension of the lower and upper black shally Kellwasser intervals. The light blue arrow marks the onset of positive carbon excursion associated with the Lower Kellwasser (372.670 ± 0.102 Ma), the dark blue arrow marks the maximum of the carbon excursion associated with the Lower Kellwasser (372.430 ± 0.102 Ma). The red dotted line marks the Frasnian–Famennian (F–F) boundary (381.870 ± 0.092 Ma).

(Fig. 6) where the age of the F–F boundary falls at 371.87 Ma, considering the 5 short eccentricity cycles between the Bed 36 bentonite and the F–F boundary. The new F–F boundary age is younger than most previous estimates (see Fig. 1). However, it is important to note that this young age is primarily inherited from the younger U–Pb age[25], rather than resulting from issues in the cyclostratigraphic framework, which conforms with previous astrochronologic studies[6]. The Lower and Upper Kellwasser black argillaceous horizons represent respectively between 80 to 96 kyr and 100 to 130 kyr of time (equivalent to approximately one short eccentricity cycle, Fig. 6, Suppl. Mat. 2). The different proxies (MS, LogTi, $\delta^{13}C$) are all in phase (Fig. 6). The interval between the onset of the Lower Kellwasser carbon-isotope excursion (372.67 Ma) and the Frasnian termination is between 690 and 843 kyr (Fig. 6, Table 1, Fig. Suppl. Mat. 2).

Uncertainty assessment on cyclostratigraphic results is a challenging endeavour[45]. An uncertainty assessment can be proposed by considering the results obtained through different cyclostratigraphy techniques and proxies, associated with the uncertainty on the ash bed. Considering the techniques applied on different proxies generates seven different cyclostratigraphic duration estimates for the studied stratigraphic interval (Table 1). The standard deviation (σ) between these techniques is 47 kyr. Since the ash bed and the cyclostratigraphic estimates are independent, the square root law combines these uncertainties (as 2σ, $2 \times \mathrm{sqrt}(\sigma 1^2 + \sigma 2^2)$). Percival et al.[25] proposed different uncertainties, one 2σ at ± 53 kyr, which represents only the measurement uncertainty and allows comparison with ash bed dates obtained through the same technique and one 2σ at ± 410 kyr, which includes the measurement, tracer and also decay constant uncertainties and must be employed when making comparisons between U–Pb ages and argon-argon (Ar–Ar) ages. Consideration of those uncertainties gives a Frasnian–Famennian boundary age of 371.870 ± 0.108 Ma for the uncertainty to be compared with other U–Pb ages and 371.870 ± 0.420 Ma to be compared with Ar–Ar ages.

The newly constructed integrated and anchored time scale obtained for the Steinbruch Schmidt section also allows for the evaluation of the impact of astronomical forcing on the Kellwasser environmental perturbations. A connection between orbital forcing and organic carbon accumulation has been frequently postulated[46–48]. However, two contrasting hypotheses exist regarding the exact nature of this link (synthesis in[49]): one in which organic matter accumulation is favoured during eccentricity maxima and one during eccentricity minima. The eccentricity maxima hypothesis involves a context of strong seasonal contrast between dry and wet seasons, allowing strong fluvial discharge, productivity blooms and organic-matter accumulation. This model is classically invoked to explain high-productivity dark sapropel layers from the Pliocene of the Mediterranean region[50,51]. The eccentricity minima hypothesis invokes a scenario of enhanced preservation, involves low seasonal contrast, associated with stable conditions, with water mass stratification allowing organic matter preservation and persistent anoxia. This model is used to explain the Cretaceous Oceanic Anoxic Events[47,48,52].

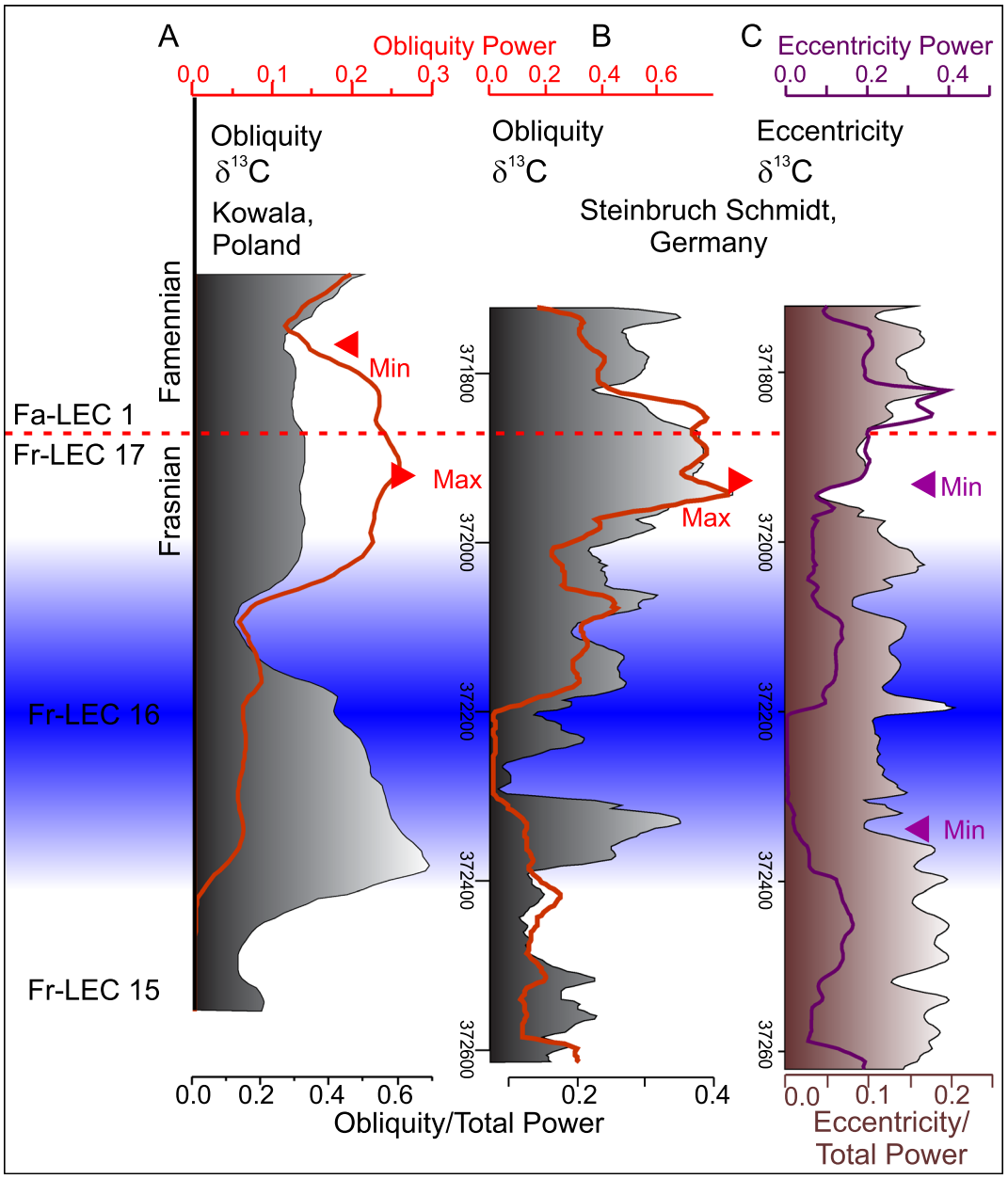

Figure 7. Changing imprint of obliquity and eccentricity forcing across lower and upper Kellwasser time scale. All analyses have been conducted using a 3–2π MTM power spectra and a 150 kyr moving window. (**A**) Obliquity power (red line) and obliquity/total power (black and grey shaded area) of the $\delta^{13}C$ record at Kowala section in Poland, by[6]. (**B**) Obliquity power (1/21 to 1/40, red line) and obliquity/total power (black and grey shaded area) of the $\delta^{13}C$ record at Steinbruch Schmidt. (**C**) Eccentricity (1/80 to 1/150, purple line) and eccentricity/total power (brown shaded area) of the $\delta^{13}C$ record at Steinbruch Schmidt. Comparison with Frasnian long eccentricity cycles (Fr-LEC) defined in[6], such as Fr-LEC 15–17 (Frasnian long Eccentricity cycle 15–17) and Fa-LEC 1 (Famennian long eccentricity cycle 1).

De Vleeschouwer et al.[6] reported maximum obliquity power in the $\delta^{13}C$ proxy starting a few tens of thousands of years before the F–F boundary. They identified that the obliquity signal is strong in this interval because it represents a 2.4 Myr minimum in eccentricity. In such an astronomical configuration, the amplitude of precession is muted, and obliquity is the dominant astronomical parameter that directly influences the distribution of insolation over the globe and over the seasons. This scenario is similar to that proposed for Cretaceous Ocean Anoxic Event 2 during the Cenomanian–Turonian interval[47,52] and fits with the eccentricity minima enhanced preservation model. The Steinbruch Schmidt section $\delta^{13}C$ proxy series tests this hypothesis. The $\delta^{13}C$ signal is long enough to includes sufficient amount of short eccentricity to focus on the evolution of obliquity and eccentricity power, to confirm or refute the minima eccentricity hypothesis.

The obliquity power of the tuned (by eTimeOpt and by ORTA) $\delta^{13}C$ record at Steinbruch Schmidt documents similar trends to those of De Vleeschouwer et al.[6], with an obliquity power reaching maximum values slightly below the F–F boundary (Fig. 7, Fig. Suppl. Mat. 3). At the same stratigraphic level, eccentricity power reaches a minimum, confirming that the two astronomical controls are indeed inversely proportional, as expected from astronomical theory. In analogy with the Cretaceous Oceanic Anoxic Events, the Steinbruch Schmidt results support an Upper Kellwasser global carbon-cycle perturbation generated by eccentricity minima model.

To summarise, both Kellwasser events occur over approximately only a single short eccentricity cycle and are initiated during the early (low-eccentricity) phase of a 405 kyr cycle. An extreme eccentricity minimum, during which a 2.4 Myr and 405 kyr minima culminated, likely initiated the Upper Kellwasser Event. This eccentricity minimum 2.4 Myr configuration potentially explains why the Upper Kellwasser appears to have been more severe than the lower Kellwasser. Such low-eccentricity configuration decreases seasonality and reduces circulation and overturns ocean basins, facilitating the accumulation of organic matter[6,47].

Conclusions

For the first time, an astrochronology is compiled for a Devonian section that also comprises a high-precision radio-isotopic date. This unique integration of chrono- and cyclostratigraphy results in a precisely time-calibrated sequence of events across the F–F boundary, well-anchored in numerical time.

The Steinbruch Schmidt section (Kellerwald, Germany) is ideal for this combined cyclostratrigraphy/absolute age approach because it is characterized by the rare combination of well-expressed dark shale Kellwasser intervals, reliable environmental proxies and a datable bentonite ash. The carbon isotopes, logTi and magnetic susceptibility series of the section provide new insight in the astronomical signature of environmental change across the F–F boundary and build a cyclostratigraphy for the transition. Both Kellwasser anoxic episodes are interpreted to have lasted for about one short eccentricity cycle and to have begun during a 405 kyr eccentricity minima. The Upper Kellwasser appears more severe in its expression as it corresponds to a 2.4 Myr minimum in eccentricity (compared to the Lower Kellwasser, which occurs at a 405 kyr minimum eccentricity). This study confirms the hypothesis put forward by[6] that obliquity, under a low-eccentricity orbit make the Earth system more prone to developing marine anoxia, helping the development of the low-oxygen Kellwasser events preceding the F–F boundary mass extinction. However, the main result of this study is a new F–F boundary age of 371.870 ± 0.108 Ma (to be compared with U–Pb ages).

This study demonstrates that even in the Palaeozoic a < 100 kyr time scale resolution is within reach when cyclostratigraphy can be combined with high-precision absolute ages. However, such chronologies can only be obtained through optimal proxy selection and multiproxy approach for robustness, careful comparison of different techniques for time-series analysis and an integrated stratigraphy approach.

Received: 21 February 2020; Accepted: 11 June 2020
Published online: 31 July 2020

References

1. Muscente, A. D. *et al.* Quantifying ecological impacts of mass extinctions with network analysis of fossil communities. *Proc. Natl. Acad. Sci. U.S.A.* **115**, 5217–5222 (2018).
2. Carmichael, S. K., Waters, J. A., Königshof, P., Suttner, T. J. & Kido, E. Paleogeography and paleoenvironments of the Late Devonian Kellwasser event: A review of its sedimentological and geochemical expression. *Glob. Planet. Change* **183**, 102984 (2019).
3. Joachimski, M. M. & Buggisch, W. Anoxic events in the late Frasnian—Causes of the Frasnian–Famennian faunal crisis?. *Geology* **21**, 675–678 (1993).
4. Joachimski, M. M. & Buggisch, W. Conodont apatite $\delta^{13}C$ signatures indicate climatic cooling as a trigger of the Late Devonian mass extinction. *Geology* **30**, 711–714 (2002).
5. Whalen, M. T. *et al.* Chemostratigraphy and magnetic susceptibility of the Late Devonian Frasnian–Famennian transition in western Canada and southern China: Implications for carbon and nutrient cycling and mass extinction. *Geol. Soc. London Spec. Publ.* **414**, 414–418 (2015).
6. De Vleeschouwer, D. *et al.* Timing and pacing of the Late Devonian mass extinction event regulated by eccentricity and obliquity. *Nat. Commun.* **8**, 2268 (2017).
7. Claeys, P., Casier, J.-G. & Margolis, S. V. Microtektites and mass extinctions: Evidence for a Late Devonian asteroid impact. *Science* **257**, 1102–1104 (1992).
8. McGhee, G. R. The 'multiple impacts hypothesis' for mass extinction: A comparison of the Late Devonian and the late Eocene. *Palaeogeogr. Palaeoclimatol. Palaeoecol.* **176**, 47–58 (2001).
9. Racki, G., Rakocinski, M., Marynowski, L. & Wignall, P. B. Mercury enrichments and the Frasnian–Famennian biotic crisis: A volcanic trigger proved?. *Geology* **46**, 543–546 (2018).
10. Racki, G. A volcanic scenario for the Frasnian–Famennian major biotic crisis and other Late Devonian global changes: More answers than questions?. *Glob. Planet. Change* **189**, 103174 (2020).
11. Joachimski, M. M., Pancost, R. D., Freeman, K. H., Ostertag-Henning, C. & Buggisch, W. Carbon isotope geochemistry of the Frasnian–Famennian transition. *Palaeogeogr. Palaeoclimatol. Palaeoecol.* **181**, 91–109 (2002).
12. Thompson, J. B. & Newton, C. R. Late Devonian mass extinction; episodic climatic cooling or warming? In *Devonian of the World* (eds McMillen, N. J. *et al.*) 29–34 (Canadian Society of Petroleum Geologists, Memoirs, Calgary, 1988).
13. Averbuch, O. *et al.* Mountain building-enhanced continental weathering and organic carbon burial as major causes for climatic cooling at the Frasnian–Famennian boundary (c. 376 Ma)?. *Terra Nov.* **17**, 25–34 (2005).
14. Algeo, J. T. & Scheckler, S. E. Terrestrial-marine teleconnections in the Devonian: Links between the evolution of land plants, weathering processes and marine anoxic events. *Philos. Trans. R. Soc. Lond.* **353**, 113–130 (1998).
15. Becker, R. T. *et al. The Devonian Period. The Geologic Time Scale 2012* vols 1–2 (F. M. Gradstein, J. G. Ogg, M. Schmitz and G. Ogg, 2012).
16. Kaufmann, B. Calibrating the Devonian time scale: A synthesis of U-Pb ID-TIMS ages and conodont stratigraphy. *Earth-Sci. Rev.* **76**, 175–190 (2006).
17. Gradstein, F. M., Ogg, J. G., Schmitz, M. D. & Ogg, G. M. *The geologic time scale* (Cambridge University Press, Cambridge, 2012).

18. Tucker, R. D. *et al.* New U-Pb zircon ages and the duration and division of Devonian time. *Earth Planet. Sci. Lett.* **158**, 175–186 (1998).
19. Kaufmann, B., Trapp, E. & Mezger, K. The numerical age of the upper Frasnian (Upper Devonian) Kellwasser Horizons: A new U-Pb Zircon date from steinbruch Schmidt (Kellerwald, Germany). *J. Geol.* **112**, 495–501 (2004).
20. Da Silva, A. C. *et al.* Refining the early Devonian time scale using Milankovitch cyclicity in Lochkovian–Pragian sediments (Prague Synform, Czech Republic). *Earth Planet. Sci. Lett.* **455**, 125 (2016).
21. Grabowski, J., Narkiewicz, M. & de Vleeschouwer, D. Forcing factors of the magnetic susceptibility signal in lagoonal and subtidal depositional cycles from the Zache mie section (Eifelian, Holy Cross Mountains, Poland). *Geol. Soc. Lond. Spec. Publ.* **414**, 414 (2015).
22. Pas, D. *et al.* Cyclostratigraphic calibration of the Famennian stage (Late Devonian, Illinois Basin, USA). *Earth Planet. Sci. Lett.* **488**, 102–114 (2018).
23. De Vleeschouwer, D. *et al.* The astronomical rhythm of Late-Devonian climate change (Kowala section, Holy Cross Mountains, Poland). *Earth Planet. Sci. Lett.* **365**, 25–37 (2013).
24. Myrow, P. M. *et al.* High-precision U–Pb age and duration of the latest Devonian (Famennian) Hangenberg event, and its implications. *Terra Nov.* **26**, 222–229 (2014).
25. Percival, L. M. E. *et al.* Precisely dating the Frasnian–Famennian boundary: Implications for the cause of the Late Devonian mass extinction. *Sci. Rep.* **8**, 9578 (2018).
26. Devleeschouwer, X., Herbosch, A. & Preat, A. Microfacies, sequence stratigraphy and clay mineralogy of a condensed deep-water section around the Frasnian/Famennian boundary (Steinbruch Schmidt, Germany). *Palaeogeogr. Palaeoclimatol. Palaeoecol.* **181**, 171–193 (2002).
27. Schindler, E. Die Kellwasser-Krise (hohe Frasne-Stufe, Ober Devon). *Gött. Arb. Geol. Paläontol.* **46**, 1–115 (1990).
28. Feist, R. & Schindler, E. Trilobites during the Frasnian Kellwasser crisis in European Late Devonian cephalopod limestones. *Cour. Forsch. Inst. Senckenb.* **169**, 195–223 (1994).
29. de Winter, N. J., Sinnesael, M., Makarona, C., Vansteenberge, S. & Claeys, P. Trace element analyses of carbonates using portable and micro-X-ray fluorescence: Performance and optimization of measurement parameters and strategies. *J. Anal. At. Spectrom.* **32**, 1211–1223 (2017).
30. Friedman, I., O'neil, J. & Cebula, G. Two new carbonate stable-isotope standards. *Geostand. Newsl.* **6**, 11–12 (1982).
31. Core Team, R. R: A language and environment for computing (2018).
32. Meyers, S. R. astrochron: An R Package for Astrochronology (2014). https://cran.r-project.org/package=astrochron. Accessed July 13, 2020.
33. Meyers, S. R. Cyclostratigraphy and the problem of astrochronologic testing. *Earth-Sci. Rev.* **190**, 190–223 (2019).
34. Meyers, S. R. The evaluation of eccentricity-related amplitude modulation and bundling in paleoclimate data: An inverse approach for astrochronologic testing and time scale optimization. *Paleoceanography* **30**, 1625–1640 (2015).
35. Berger, A., Loutre, M. F. & Laskar, J. Stability of the astronomical frequencies over the earth's history for paleoclimate studies. *Science* **255**, 560–566 (1992).
36. Laskar, J. *et al.* A long-term numerical solution for the insolation quantities of the Earth. *Astron. Astrophys.* **428**, 261–285 (2004).
37. Laskar, J., Fienga, A., Gastineau, M. & Manche, H. La2010: A new orbital solution for the long term motion of the Earth. *Astron. Astrophys.* **89**, 1–15 (2011).
38. Torrence, C. & Compo, G. P. A practical guide to wavelet analysis. *Bull. Am. Meteorol. Soc.* **79**, 61–78 (1998).
39. Gouhier, T. C., Grinsted, A. & Viliam, S. R Package biwavelet: Conduct Univariate and Bivariate Wavelet Analyses (2018).
40. Da Silva, A. C. *et al.* Magnetic susceptibility as a high-resolution correlation tool and as a climatic proxy in Paleozoic rocks—Merits and pitfalls: Examples from the Devonian in Belgium. *Mar. Pet. Geol.* **46**, 173 (2013).
41. Calvert, S. E. & Pedersen, T. F. Chapter fourteen elemental proxies for palaeoclimatic and palaeoceanographic variability in marine sediments: Interpretation and application. *Dev. Mar. Geol.* **1**, 567–644 (2007).
42. Murphy, A. E., Sageman, B. B., Hollander, D. J., Lyons, T. W. & Brett, C. E. Black shale deposition and faunal overturn in the Devonian Appalachian basin: Clastic starvation, seasonal water-column mixing, and efficient biolimiting nutrient recycling. *Paleoceanography* **15**, 280–291 (2000).
43. Kump, L. R. & Arthur, M. A. Interpreting carbon-isotope excursions: Carbonates and organic matter. *Chem. Geol.* **161**, 181–198 (1999).
44. Wignall, P. B. Model for transgressive black shales?. *Geology* **19**, 167–170 (1991).
45. Sinnesael, M. *et al.* The cyclostratigraphy intercomparison project (CIP): Consistency, merits and pitfalls. *Earth-Sci. Rev.* **199**, 102965 (2019).
46. Herbert, T. D. & Fischer, A. G. Milankovitch climatic origin of mid-Cretaceous black shale rhythms in central Italy. *Nature* **321**, 739–743 (1986).
47. Meyers, S. R., Sageman, B. B. & Arthur, M. A. Obliquity forcing of organic matter accumulation during oceanic anoxic event 2. *Paleoceanography* **27**, 1–19 (2012).
48. Mitchell, R. N. *et al.* Oceanic anoxic cycles? Orbital prelude to the Bonarelli level (OAE 2). *Earth Planet. Sci. Lett.* **267**, 1–16 (2008).
49. Gambacorta, G., Menichetti, E., Trincianti, E. & Torricelli, S. Orbital control on cyclical primary productivity and benthic anoxia: Astronomical tuning of the Telychian stage (Early Silurian). *Palaeogeogr. Palaeoclimatol. Palaeoecol.* **495**, 152–162 (2018).
50. Hilgen, F. J. *et al.* Extending the astronomical (polarity) time scale into the Miocene. *Earth Planet. Sci. Lett.* **136**, 495–510 (1995).
51. Rohling, E. J., Marino, G. & Grant, K. M. Mediterranean climate and oceanography, and the periodic development of anoxic events (sapropels). *Earth-Sci. Rev.* **143**, 62–97 (2015).
52. Batenburg, S. J. *et al.* Orbital control on the timing of oceanic anoxia in the Late Cretaceous. *Clim. Past* **12**, 2009–2016 (2016).
53. De Vleeschouwer, D. & Parnell, A. C. Reducing time-scale uncertainty for the devonian by integrating astrochronology and bayesian statistics. *Geology* **42**, 491–494 (2014).
54. Blakey, R. C. Global Paleogeography. https://deeptimemaps.com/global-paleogeography-and-tectonics-in-deep-time-series/ (2016). Accessed July 13, 2020.
55. De Vleeschouwer, D., Whalen, M. T., Day, J. E. & Claeys, P. Cyclostratigraphic calibration of the Frasnian (Late Devonian) timescale (Western Alberta, Canada). *Geol. Soc. Am. Bull.* **124**, 928–942 (2012).

Acknowledgements

We acknowledge the owner of the Steinbruch Schmidt quarry for allowing us access. A.-C.D.S. acknowledges the FNRS Grant (PDR T.0051.19). M.S. thanks the Research Foundation of Flanders (FWO) for the awarded Ph.D. fellowship (FWOTM782). N.J.d.W. acknowledges funding by the Flemish Research Council (FWO; IWT700). The micro-XRF and Nu-Instrument stable isotope platforms at the VUB were supported by FWO Hercules grants to Ph.C. Ph.C. also thanks the VUB strategy research for continuous funding of this research topic. This paper is part of the IGCP-652 project.

Author contributions

A.-C.D.S. and D.D.V. designed the study, made the measurements and interpreted the data. A.-C.D.S. wrote the manuscript, with significant input from Ph.C. and D.D.V.; M.S. measured and interpreted the data; Ph.C., J.H.F.L.D., N.J.d.W., L.P. and U.S. helped for the interpretations. All Authors reviewed the manuscript.

Competing interests

The authors declare no competing interests.

Additional information

Supplementary information is available for this paper at https://doi.org/10.1038/s41598-020-69097-6.

Correspondence and requests for materials should be addressed to A.-C.D.S. or D.D.V.

Reprints and permissions information is available at www.nature.com/reprints.

Publisher's note Springer Nature remains neutral with regard to jurisdictional claims in published maps and institutional affiliations.